

# Two dark matter candidates in a doublet-triplet Higgs model

S. Melara-Duron<sup>1,2\*</sup>, R. Gaitán<sup>3</sup> and J. M. Lamprea<sup>3</sup>

<sup>1\*</sup>Instituto de Física, Universidad Nacional Autónoma de México, A.P. 20-364, Ciudad de México, 01000, México.

<sup>2\*</sup>Departamento de Astronomía y Astrofísica, Facultad de Ciencias Espaciales, Universidad Nacional Autónoma de Honduras, Bulevar Suyapa, Tegucigalpa, M.D.C., Honduras.

<sup>3</sup>Departamento de Física, Facultad de Estudios Superiores Cuautitlán, Universidad Nacional Autónoma de México, Estado de México, 54770, México.

\*Corresponding author(s). E-mail(s): [sheryl.melara@unah.edu.hn](mailto:sheryl.melara@unah.edu.hn);  
Contributing authors: [rgaitan@unam.mx](mailto:rgaitan@unam.mx); [jmlamprea@gmail.com](mailto:jmlamprea@gmail.com);

## Abstract

We study a Standard Model extension that provides a bicomponent dark matter scenario as well as a mechanism for the generation of left-handed neutrino masses. We extend the Standard Model scalar sector by adding an inert  $SU(2)_L$  doublet with hypercharge  $\mathbf{Y} = \mathbf{1}/2$  and a triplet with hypercharge  $\mathbf{Y} = \mathbf{0}$ . These scalars provide dark matter candidates in two dark sectors stabilised by discrete symmetries. We consider the contribution of both candidates to the total relic abundance in order to recover the desert regions in their standard alone cases. In addition, we add an active scalar  $SU(2)_L$  triplet with hypercharge  $\mathbf{Y} = \mathbf{1}$  in order to generate light neutrino masses. We analyse the results of dark matter phenomenology for the model and the neutrino mass generation through the type-II seesaw mechanism.

**Keywords:** scalar dark matter, beyond Standard Model, WIMPs, multi-Higgs models

# 1 Introduction

The Standard Model (SM) of particle physics successfully explains most particle phenomena we observe in Nature [1–3]. However, the SM cannot provide an explanation to some anomalies found in the Universe. Among those puzzles are: the origin of light neutrino masses [4], the mechanism behind the origin of the matter-antimatter asymmetry and the existence of dark matter (DM) [5]. In spite of the fact that it has not been possible yet to detect DM, direct detection experiments impose upper bounds on the cross-section for DM-nucleon interactions. The current most stringent limits are set by, PANDAX-II [6], LUX-ZEPLIN [7] and XENONnT [8] experiments. DM candidates must satisfy those experimental constraints as well as theoretical ones [9].

In order to describe DM and its interactions with ordinary matter, we need to go beyond the Standard Model (BSM). The most studied BSM scenario includes particles like WIMPs (Weakly Interactive Massive Particles) as DM candidates. One of the most popular of those extensions is the Inert Doublet Model (IDM) [10–13], which consists of adding to the SM content an inert scalar  $SU(2)_L$  doublet. This model provides a good DM candidate for the mass region  $M_{DM} \geq 550$  GeV. However, for smaller mass values,  $M_W < M_{DM} < 550$  GeV, the relic density of the DM turns to be under-abundant<sup>1</sup> due to the large annihilation cross-section of dark matter in that region. Another successful model is the Scotogenic model proposed by Ernest Ma [14]. This model, in addition to provide a good dark matter candidate as the IDM, also provides a mechanism to generate light neutrino masses at the radiative level. However, it also has the same under-abundant region as the IDM. In addition to the Inert Doublet and Scotogenic models, other scalar DM models have been proposed, such as singlet and triplet extensions [15]. Here we are interested in Inert Triplet Models (ITM) [16, 17] which postulate a scalar DM candidate as well, though a wider desert region:  $M < 1970$  GeV is observed compared to the IDM.

A possible solution to the problem of under-abundance in the IDM and ITM is considering the contribution of two DM candidates to account for the total relic density. Two-component DM scenarios have recently become a topic of interest [18, 19]. In this work, we study an extension of the SM with two dark sectors. We consider the neutral CP even component of a  $SU(2)_L$  scalar doublet and the neutral component of a  $SU(2)_L$  scalar triplet as our DM candidates. Provided that some DM mass regions are forbidden in each case separately, we aim to study DM-DM conversion between the two candidates to recover some of those regions. Additionally, to the study of DM phenomenology, we include an active triplet  $\Delta$  with hypercharge  $Y = 1$  to generate the light neutrino masses via the seesaw type-II mechanism. It is worth to mention that models with triplets have received attention since it is possible to generate baryogenesis via leptogenesis through the decay of heavy particles.

This paper is organised as follows. In the first section 2, we introduced our two dark sector model where dark matter candidates are both scalars. In section 3, we present the neutrino mass generation through the seesaw type-II mechanism. Section 4 discusses the relevant constraints in our model. Our results for DM phenomenology are presented and discussed in section 5. Finally, we present our conclusions in section 6.

---

<sup>1</sup>This is often referred as the desert region.

## 2 The Model

Particle	$SU(2)_L$	$U(1)_Y$	$\mathbb{Z}_2$	$\mathbb{Z}'_2$
$\Phi_1$	<b>2</b>	1/2	+	+
$\Phi_2$	<b>2</b>	1/2	-	+
$\Delta$	<b>3</b>	1	+	+
$T$	<b>3</b>	0	+	-

**Table 1:** Quantum numbers of the relevant particles in the model.

In the present study, we have considered an extension of the SM where we have included a complex scalar  $SU(2)_L$  doublet  $\Phi_2$  with  $Y = 1/2$ , a real scalar  $SU(2)_L$  triplet  $T$  with hypercharge  $Y = 0$  and a real scalar  $SU(2)_L$  triplet  $\Delta$  with hypercharge  $Y = 1$ . Our dark matter candidates come from the lightest neutral CP-even components of doublet  $\Phi_2$  and triplet  $T$ . The stability of the DM candidate is guaranteed by the direct product of discrete  $Z_2$  symmetries  $\mathbb{Z}_2 \times \mathbb{Z}'_2$ . All the SM fields are trivially charged under this symmetry, while  $\Phi_2$  and  $T$  belong to each dark sector  $Z_2$  and  $Z'_2$  respectively.

The relevant particle content and quantum numbers of the added fields in the model are described in Table 1. The most general scalar potential renormalisable and invariant under the SM gauge and  $\mathbb{Z}_2 \times \mathbb{Z}'_2$  symmetry can be written as:

$$V = V_{\Phi_1\Phi_2} + V_\Delta + V_T + V_{\text{int}}, \quad (1)$$

where,

$$V_{\Phi_1\Phi_2} = \mu_1^2 \Phi_1^\dagger \Phi_1 + \lambda_1 (\Phi_1^\dagger \Phi_1)^2 + \mu_2^2 \Phi_2^\dagger \Phi_2 + \lambda_2 (\Phi_2^\dagger \Phi_2)^2 + \lambda_3 \Phi_1^\dagger \Phi_1 \Phi_2^\dagger \Phi_2 + \lambda_4 \Phi_1^\dagger \Phi_2 \Phi_2^\dagger \Phi_1 + \frac{1}{2} \lambda_5 \left[ (\Phi_1^\dagger \Phi_2)^2 + (\Phi_2^\dagger \Phi_1)^2 \right], \quad (2)$$

$$V_\Delta = \mu_\Delta^2 \Delta^\dagger \Delta + \lambda_\Delta (\Delta^\dagger \Delta)^2, \quad (3)$$

$$V_T = \mu_T^2 T^\dagger T + \lambda_T (T^\dagger T)^2, \quad (4)$$

$$V_{\text{int}} = \kappa_{\Phi_1\Delta} \left( \Phi_1^\dagger \Delta \tilde{\Phi}_1 + h.c. \right) + \kappa_{\Phi_2\Delta} \left( \Phi_2^\dagger \Delta \tilde{\Phi}_2 + h.c. \right) + \lambda_{\Phi_1\Delta} \Phi_1^\dagger \Phi_1 \Delta^\dagger \Delta + \lambda_{\Phi_2\Delta} \Phi_2^\dagger \Phi_2 \Delta^\dagger \Delta + \lambda_{\Phi_1 T} \Phi_1^\dagger \Phi_1 T^\dagger T + \lambda_{\Phi_2 T} \Phi_2^\dagger \Phi_2 T^\dagger T. \quad (5)$$

We consider all the parameters in the scalar potential to be real. We also consider  $\mu_1^2 < 0$  as required by the Electroweak Symmetry Breaking (EWSB). The scalar fields can be parametrised as

$$\Phi_1 = \begin{pmatrix} 0 \\ \frac{v+h}{\sqrt{2}} \end{pmatrix}, \quad \Phi_2 = \begin{pmatrix} H^+ \\ \frac{H^0 + iA^0}{\sqrt{2}} \end{pmatrix}, \quad (6)$$

$$\Delta = \begin{pmatrix} \frac{\Delta^+}{\sqrt{2}} & \Delta^{++} \\ v_\Delta + \Delta^0 & -\frac{\Delta^+}{\sqrt{2}} \end{pmatrix}, \quad T = \begin{pmatrix} \frac{T^0}{\sqrt{2}} & -T^+ \\ -T^- & -\frac{T^0}{\sqrt{2}} \end{pmatrix}. \quad (7)$$

The Vacuum Expectation Values (VEV) of the fields  $\Phi_1$  and  $\Delta$  are labeled as  $v$  and  $v_\Delta$  respectively. On the other hand, the fields  $\Phi_2$  and  $T$  do not pick up a VEV as they are inert fields. The masses of the physical scalars after EWSB are:

$$m_h^2 = 2\lambda_1 v^2, \quad (8)$$

$$m_{H^\pm}^2 = \mu_2^2 + \frac{1}{2}\lambda_3 v^2 + \lambda_{\Phi_2\Delta} v_\Delta^2, \quad (9)$$

$$m_{H^0}^2 = \mu_2^2 + \frac{1}{2}(\lambda_3 + \lambda_4 + \lambda_5) v^2 + \mu_{\Phi_2\Delta} v_\Delta + \lambda_{\Phi_2\Delta} v_\Delta^2, \quad (10)$$

$$m_{A^0}^2 = \mu_2^2 + \frac{1}{2}(\lambda_3 + \lambda_4 - \lambda_5) v^2 - \mu_{\Phi_2\Delta} v_\Delta + \lambda_{\Phi_2\Delta} v_\Delta^2, \quad (11)$$

$$m_{T^\pm, T^0}^2 = \mu_T^2 + \frac{1}{2}\lambda_{\Phi_1 T} v^2, \quad (12)$$

$$m_{\Delta^{\pm\pm}}^2 = -\frac{1}{2}\kappa_{\Phi_1\Delta} \frac{v^2}{v_\Delta}, \quad (13)$$

$$m_{\Delta^\pm, \Delta^0}^2 = -\frac{1}{4}\kappa_{\Phi_1\Delta} \frac{v^2}{v_\Delta}, \quad (14)$$

where  $\kappa_{\Phi_1\Delta} < 0$  and  $v = 246$  GeV. We identify  $m_h = 125.09$  GeV [20] as the mass of the SM Higgs boson. Without any loss of generality, we choose  $\lambda_5 < 0$  so that the CP even component of  $\Phi_2$ ,  $H_0$  is the lightest  $Z_2$  odd particle and therefore, a DM candidate. Our second DM candidate is the lightest  $Z_2'$  odd particle,  $T_0$ . We observe that the mass difference between the charged  $H^\pm$  and CP-even component  $H_0$  of the inert doublet,  $m_{H^\pm} - m_{H^0}$  and  $m_{A^0} - m_{H^0}$  are free parameters in the model. On the contrary, the charged and neutral components of the inert triplet  $T$  have degenerate masses at tree level. However, due to radiative effects, there is a mass splitting at one-loop level [21]

$$\Delta m_T = m_{T^\pm} - m_{T^0} = 166 \text{ MeV}. \quad (15)$$

The relevant parameters in our model for relic density calculation are five masses  $m_{H^0}$ ,  $m_{H^\pm}$ ,  $m_{A^0}$ ,  $m_{T^0}$ ,  $m_{T^\pm}$ , and three quartic couplings  $\lambda_L$ ,  $\lambda_{\Phi_1 T}$ ,  $\lambda_{\Phi_2 T}$ , where we have defined

$$\lambda_L = \frac{1}{2}(\lambda_3 + \lambda_4 + \lambda_5), \quad (16)$$

as an independent parameter.

We will restrict the value of these parameters in section 4 using the respective theoretical and experimental constraints.

### 3 Neutrino Masses

The Yukawa part of the Lagrangian involved in the Left Handed (LH) neutrino mass generation is given by

$$\mathcal{L}_Y = Y_\Delta^{\alpha\beta} L_\alpha^T C i\tau_2 \Delta L_\beta + h.c., \quad (17)$$

where  $\alpha, \beta$  correspond to flavour indices,  $C$  is the Charge conjugation operator,  $\tau_2$  is the second Pauli matrix,  $\tilde{\Phi}_2 = i\tau_2 \Phi_2^*$  and  $L_\alpha = (\nu_\alpha, \ell_{L\alpha})$  is the LH lepton doublet  $\alpha$ .

Due to the presence of the active triplet  $\Delta$ , the LH neutrino masses are generated through the seesaw type-II [22] mechanism:

$$m_\nu^{II} = \kappa_{\Phi_1\Delta} \frac{v^2}{M_\Delta^2} Y_\Delta, \quad (18)$$

where  $Y_\Delta$  is the Yukawa coupling matrix of the triplet  $\Delta$  with leptons. The VEV of the triplet is related to the VEV of Higgs through:  $v_\Delta \simeq \kappa_{\Phi_1\Delta} v^2 / 2M_\Delta^2$ . Therefore, we obtain:

$$m_\nu^{II} = 2v_\Delta Y_\Delta. \quad (19)$$

According to the type-II seesaw equation (18), the mass of the scalar triplet  $\Delta$  must be large enough to generate the correct left-handed neutrino masses. In addition, the VEV of the triplet must be very small [23]. For that reason we have chosen  $M_\Delta = 1$  TeV and  $v_\Delta = 1$  eV.

We can adjust the Yukawa coupling matrix  $Y_\Delta$  in  $m_\nu^{II}$  to produce the light neutrino masses according to neutrino oscillation data. Hence, we consider:

$$m_\nu^{II} = U^* m_\nu^d U^\dagger, \quad (20)$$

where  $m_\nu^d = \text{diag}(m_1, m_2, m_3)$  and  $U$  is the Pontecorvo–Maki–Nakagawa–Sakata (PMNS) neutrino mixing matrix, parametrised as

$$U = \begin{pmatrix} c_{12} c_{13} & s_{12} c_{13} & s_{13} e^{-i\delta_{CP}} \\ -s_{12} c_{23} - c_{12} s_{13} s_{23} e^{i\delta_{CP}} & c_{12} c_{23} - s_{12} s_{13} s_{23} e^{i\delta_{CP}} & c_{13} s_{13} \\ s_{12} s_{13} - c_{12} s_{13} c_{23} e^{i\delta_{CP}} & -c_{12} s_{23} - s_{12} s_{13} c_{23} e^{i\delta_{CP}} & c_{13} c_{23} \end{pmatrix}, \quad (21)$$

where  $c_{ij} \equiv \cos \theta_{ij}$ ,  $s_{ij} \equiv \sin \theta_{ij}$  and  $\delta_{CP}$  is the Dirac CP violation phase. We use the best-fit values of the neutrino mixing angles and CP phase according to [24]. For simplicity, we consider  $m_1 = 0$  in the case of Normal mass Ordering (NO) and  $m_3 = 0$  for Inverted mass Ordering (IO), as well as the Majorana phases to be zero. For the NO we obtain the following Yukawa coupling matrix

$$Y_\Delta = 10^{-3} \times \begin{pmatrix} 1.361 + 0.560i & -0.646 - 1.956i & -3.208 - 1.742i \\ -0.646 - 1.956i & 15.221 - 0.214i & 10.697 + 0.008i \\ -3.208 - 1.742i & 10.697 + 0.008i & 12.300 + 0.185i \end{pmatrix}. \quad (22)$$

In the same way, for the IO we obtain

$$Y_{\Delta} = 10^{-3} \times \begin{pmatrix} 24.228 & -0.603 - 2.671i & -0.758 - 2.354i \\ -0.603 - 2.671i & 10.623 + 0.134i & -12.607 + 0.142i \\ -0.758 - 2.354i & -12.607 + 0.142i & 13.822 + 0.147i \end{pmatrix}. \quad (23)$$

## 4 Constraints

In the following, we discuss the theoretical and experimental constraints imposed on the numerical scan.

### 4.1 Experimental Constraints

#### 4.1.1 Dark Matter Abundance

In order to provide appropriate DM candidates, our model must be able to yield the right DM abundance according to Cosmological observations. From the latest Planck Collaboration [25] data analysis, the DM relic abundance should be within the range

$$\Omega_{DM} h^2 = 0.1200 \pm 0.0010. \quad (24)$$

We have imposed the restriction that our results for the total relic density must lie within that band. In addition, we have included the most updated upper limits for the Spin-Independent (SI) cross-section from direct detection experiments. We used the limits set by PANDAX-II [6], LUX-ZEPLIN [7] and XENONnT [8] which are currently the most stringent limits.

#### 4.1.2 Constrictions from Colliders

The absence of a signal within searches of supersymmetric neutralinos can be used to constrain the IDM in the LEP II [26, 27]; data analysis excludes the mass regions:

$$m_{H^0} < 80 \text{ GeV}, \quad m_{A^0} < 100 \text{ GeV} \quad \text{and} \quad \Delta m = m_{A^0} - m_{H^0} > 8 \text{ GeV}. \quad (25)$$

The search of charginos from OPAL [28] collaboration imposes the following bounds for the charged Higgs masses [29]:

$$m_{H^{\pm}} \gtrsim 70 - 90 \text{ GeV}. \quad (26)$$

Additionally, the LHC [30] sets constraints on the mass of the active scalar triplet  $\Delta$  components:

$$m_{\Delta^{\pm\pm}} > 820 \text{ GeV} \text{ and } m_{\Delta^{\pm}} > 350 \text{ GeV}. \quad (27)$$

### 4.2 Theoretical Constraints

#### 4.2.1 Positivity and stability of the scalar potential

To ensure the potential remains stable and bounded from below, we need to determine the necessary vacuum stability conditions. Applying co-positivity criteria [31], we have

obtained for the quartic couplings

$$\lambda_1 > 0, \quad \lambda_2 > 0, \quad \lambda_\Delta > 0, \quad \lambda_T > 0, \quad (28)$$

and

$$\lambda_3 + \lambda_4 - |\lambda_5| + \sqrt{\lambda_1 \lambda_2} > 0, \quad \lambda_3 + \sqrt{\lambda_1 \lambda_2} > 0, \quad (29)$$

$$\lambda_{\Phi_1 \Delta} + \sqrt{\lambda_1 \lambda_4} > 0, \quad \lambda_{\Phi_2 \Delta} + \sqrt{\lambda_2 \lambda_\Delta} > 0, \quad (30)$$

$$\lambda_{\Phi_1 T} + \sqrt{\lambda_1 \lambda_T} > 0, \quad \lambda_{\Phi_2 T} + \sqrt{\lambda_2 \lambda_T} > 0. \quad (31)$$

### 4.2.2 Unitarity

Additionally, we must consider the restrictions coming from the unitarity [32] of the scattering matrix. Unitarity demands the absolute eigenvalues of the scattering matrix to be less than  $8\pi$ . Imposing that constraint in our model we obtain:

$$|\lambda_3 \pm \lambda_4| \leq 8\pi, \quad |\lambda_3 \pm \lambda_5| \leq 8\pi, \quad |\lambda_3 + 2\lambda_4 \pm \lambda_5| \leq 8\pi,$$

$$|\lambda_T| \leq 24\pi, \quad |\lambda_\Delta| \leq 24\pi, \quad |\lambda_{\Phi_2 T}| \leq 8\pi, \quad (32)$$

$$|\lambda_{\Phi_1 T}| \leq 8\pi, \quad |\lambda_{\Phi_1 \Delta}| \leq 8\pi, \quad |\lambda_{\Phi_2 \Delta}| \leq 8\pi,$$

$$\left| \lambda_1 + \lambda_2 \pm \sqrt{(\lambda_1 - \lambda_2)^2 + \lambda_4^2} \right| \leq 8\pi, \quad \left| \lambda_1 + \lambda_2 \pm \sqrt{(\lambda_1 - \lambda_2)^2 + \lambda_5^2} \right| \leq 8\pi.$$

### 4.2.3 Perturbativity

Perturbativity of the scalar potential requires the parameters of the model must satisfy:

$$|\lambda_i| \leq 4\pi, \quad |g_i|, |y_{\alpha\beta}| \leq \sqrt{4\pi}, \quad (33)$$

where  $\lambda_i$  are the quartic couplings, while  $g_i$  and  $y_{\alpha\beta}$  denote the SM gauge and Yukawa couplings respectively.

### 4.2.4 Oblique parameters

Adding new fields to the Standard Model Lagrangian induces a contribution to the oblique parameters  $S, T, U$  [33]. For  $X = S, T, U$ , we can write this contribution as

$$\Delta X = \Delta X_{ID} + \Delta X_{IT} + \Delta X_{AT}, \quad (34)$$

where the subscripts ID, IT and AT denote the contribution from the inert doublet  $H$ , inert triplet  $T$  and active triplet  $\Delta$  respectively.

In the case of the inert doublet, we obtain [34]

$$\begin{aligned} \Delta S_{ID} = & \frac{1}{2\pi} \left[ \frac{1}{6} \log \left( \frac{m_{H^0}^2}{m_{H^\pm}^2} \right) - \frac{5}{36} + \frac{m_{H^0}^2 m_{A^0}^2}{3(m_{A^0}^2 - m_{H^0}^2)^2} \right] \\ & + \frac{1}{2\pi} \left[ \frac{m_{A^0}^4 (m_{A^0}^2 - 3m_{H^0}^2)}{6(m_{A^0}^2 - m_{H^0}^2)^3} \log \left( \frac{m_{A^0}^2}{m_{H^0}^2} \right) \right], \end{aligned} \quad (35)$$

$$\Delta T_{ID} = \frac{1}{16\pi s_W^2 M_W^2} [F(m_{H^+}^2, m_{H^0}^2) + F(m_{H^+}^2, m_{A^0}^2) - F(m_{H^0}^2, m_{A^0}^2)], \quad (36)$$

$$\Delta U_{ID} = 0. \quad (37)$$

where, the  $F(x, y)$  function is given by

$$F(x, y) = \begin{cases} \frac{x+y}{2} - \frac{xy}{x-y} \log\left(\frac{x}{y}\right), & \text{for } x \neq y, \\ 0, & \text{for } x = y. \end{cases} \quad (38)$$

For the inert triplet [35]

$$\Delta S_{IT} = 0, \quad (39)$$

$$\Delta T_{IT} = \frac{1}{8\pi s_W^2 M_W^2} \left[ m_{T^+}^2 + m_{T^0}^2 - \frac{2m_{T^+}^2 m_{T^0}^2}{m_{T^+}^2 - m_{T^0}^2} \log\left(\frac{m_{T^+}^2}{m_{T^0}^2}\right) \right], \quad (40)$$

$$\begin{aligned} \Delta U_{IT} = & -\frac{1}{3\pi} \left[ m_{T^+}^2 \log\left(\frac{m_{T^+}^2}{m_{T^0}^2}\right) \frac{3m_{T^0}^2 - m_{T^+}^2}{(m_{T^+}^2 - m_{T^0}^2)^3} \right] \\ & - \frac{1}{3\pi} \left[ \frac{5(m_{T^+}^4 + m_{T^0}^4) - 22m_{T^+}^2 m_{T^0}^2}{6(m_{T^+}^2 - m_{T^0}^2)^2} \right]. \end{aligned} \quad (41)$$

Finally, for the active triplet, we obtain [36]:

$$\begin{aligned} \Delta S_{AT} = & -\frac{1}{3\pi} \log\left(\frac{m_{\Delta^{++}}^2}{m_{\Delta^0}^2}\right) - \frac{2}{\pi} \left[ (1 - 2s_W^2)^2 \xi\left(\frac{m_{\Delta^{++}}^2}{m_Z^2}, \frac{m_{\Delta^{++}}^2}{m_Z^2}\right) \right] \\ & - \frac{2}{\pi} \left[ s_W^4 \xi\left(\frac{m_{\Delta^+}^2}{m_Z^2}, \frac{m_{\Delta^+}^2}{m_Z^2}\right) + \xi\left(\frac{m_{\Delta^0}^2}{m_Z^2}, \frac{m_{\Delta^0}^2}{m_Z^2}\right) \right], \end{aligned} \quad (42)$$

$$\Delta T_{AT} = \frac{1}{4\pi s_W^2 M_W^2} [F(m_{\Delta^{++}}^2, m_{\Delta^+}^2) + F(m_{\Delta^+}^2, m_{\Delta^0}^2)], \quad (43)$$

$$\begin{aligned} \Delta U_{AT} = & \frac{1}{6\pi} \log\left(\frac{m_{\Delta^+}^4}{m_{\Delta^{++}}^2 m_{\Delta^0}^2}\right) \\ & + \frac{2}{\pi} \left[ (1 - 2s_W^2)^2 \xi\left(\frac{m_{\Delta^{++}}^2}{m_Z^2}, \frac{m_{\Delta^{++}}^2}{m_Z^2}\right) + s_W^4 \xi\left(\frac{m_{\Delta^+}^2}{m_Z^2}, \frac{m_{\Delta^+}^2}{m_Z^2}\right) + \xi\left(\frac{m_{\Delta^0}^2}{m_Z^2}, \frac{m_{\Delta^0}^2}{m_Z^2}\right) \right] \\ & - \frac{2}{\pi} \left[ \xi\left(\frac{m_{\Delta^{++}}^2}{m_W^2}, \frac{m_{\Delta^+}^2}{m_W^2}\right) + \xi\left(\frac{m_{\Delta^+}^2}{m_Z^2}, \frac{m_{\Delta^0}^2}{m_Z^2}\right) \right]. \end{aligned} \quad (44)$$

Where the functions are defined as follows:

$$\begin{aligned} \xi(x, y) = & \frac{4}{9} - \frac{5}{12}(x+y) + \frac{1}{6}(x-y)^2 + \frac{1}{4} \left[ x^2 - y^2 - \frac{1}{3}(x-y)^3 - \frac{x^2 + y^2}{x-y} \right] \log\left(\frac{x}{y}\right) \\ & - \frac{1}{12} d(x, y) f(x, y) \end{aligned}$$



$$d(x, y) = -1 + 2(x + y) - (x - y)^2$$

$$f(x, y) = \begin{cases} -2\sqrt{d(x, y)} \left[ \arctan \frac{x - y + 1}{\sqrt{d(x, y)}} - \arctan \frac{x - y - 1}{\sqrt{d(x, y)}} \right], & d(x, y) > 0 \\ \sqrt{-d(x, y)} \log \left( \frac{x + y - 1 + \sqrt{-d(x, y)}}{x + y - 1 - \sqrt{-d(x, y)}} \right), & d(x, y) \leq 0 \end{cases}$$

We have performed a numerical scan of the contribution to the oblique parameters  $S$ ,  $T$  and  $U$  of every field in our model. Considering the experimental constraints on the masses of the scalars, we have used random values within the ranges:  $100 \leq m_{H^0} \leq 1000$  GeV for the complex inert doublet,  $100 \leq m_{T^0} \leq 2500$  GeV for the real inert triplet and  $850 \leq m_{\Delta^0} \leq 3500$  GeV for the real active triplet. For the mass splittings between the charged and neutral components we chose:  $m_{H^\pm} - m_{H^0} = m_{A^0} - m_{H^0} = 1$  GeV and  $m_{\Delta^{\pm\pm}} - m_{\Delta^\pm} = m_{\Delta^\pm} - m_{\Delta^0} = 10$  GeV. As we mentioned before, for the inert triplet  $\Delta m = 166$  MeV.

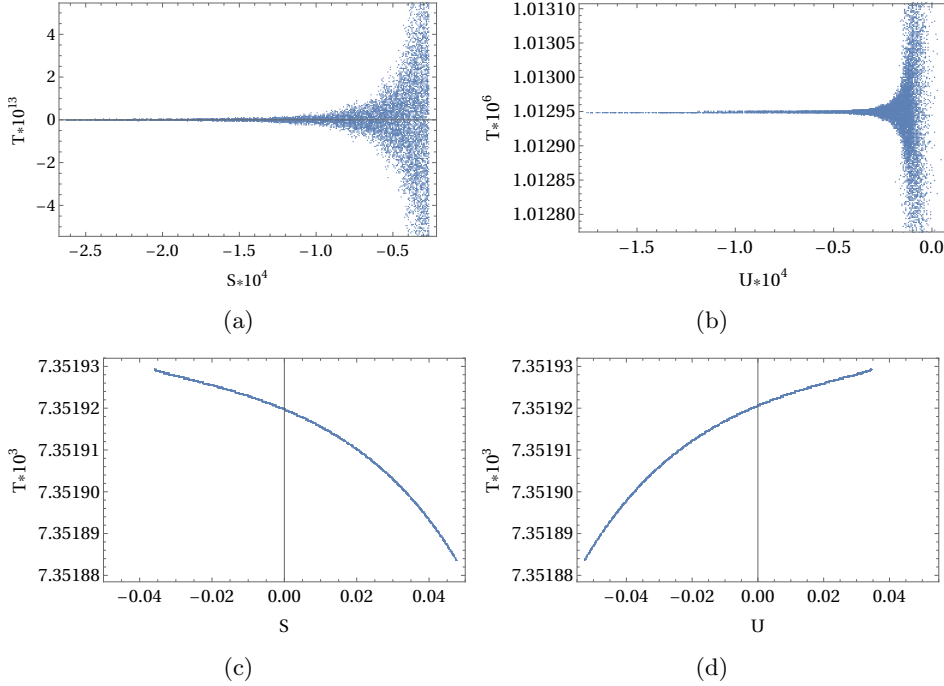


**Fig. 1:** Contribution to the oblique parameters  $S, T$  and  $U$  for (a) Inert doublet, (b) Inert triplet, (c) Active triplet and (d) Active triplet

We show in Figure 1 the results for the  $S, T$  and  $U$  parameters for each field, which lie within the most updated bounds [24]:

$$\Delta S = -0.02 \pm 0.10, \quad (45)$$

$$\Delta T = 0.03 \pm 0.12, \quad (46)$$

$$\Delta U = 0.01 \pm 0.11. \quad (47)$$

It is worth to notice that the biggest contribution comes from the real active triplet, while the contribution of the inert fields are practically negligible in comparison. Therefore, the whole the mass spectra range of the scalar fields considered is safely allowed by the bounds to the total  $S, T$  and  $U$  parameters.

## 5 Results

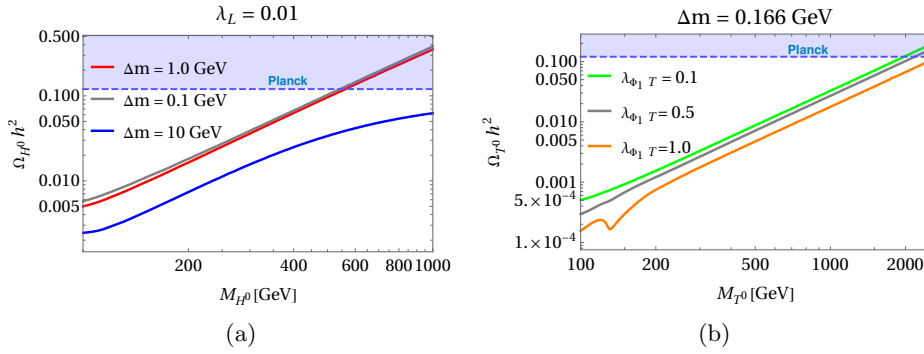


**Fig. 2:** Relic density in the IDM and ITM models. The dashed line shows the Planck limit [25] for the DM abundance

As we mention in section 2, the relevant parameters in the model are:  $m_{H^0}, m_{H^\pm}, m_{A^0}, m_{T^0}, m_{T^\pm}, \lambda_L, \lambda_{\Phi_1 T}$  and  $\lambda_{\Phi_2 T}$ . The other parameters do not have an important role in the relic density calculation; consequently, we have fixed them in the following manner:  $\lambda_{\Phi_1 \Delta} = \lambda_{\Phi_2 \Delta}, \lambda_\Delta = 0.01, \lambda_T = 0.1, m_{\Delta^0} = 1000$  GeV,  $m_{\Delta^{\pm\pm}} - m_{\Delta^\pm} = m_{\Delta^\pm} - m_{\Delta^0} = 10$  GeV and  $\kappa_{\Phi_1 \Delta} = \kappa_{\Phi_2 \Delta} \simeq 10^{-5}$  GeV. To perform our analysis we have used the following computer tools: SARAH [37] to define our model and MicrOMEGAs [38] to compute the dark matter relic abundance and Spin-Independent DM nucleon cross-section of each candidate.

### 5.1 Relic Density

First, we have computed the relic abundance for the inert doublet and the inert triplet for the standalone case in figure 2. The left panel displays the relic density for the inert doublet as a function of the DM candidate mass ( $H_0$ ). In this case, we have plotted the

relic density for different values of the mass splitting  $\Delta m$  between the scalars  $A_0$  and  $H_0$ . We observe that the desert region extends to 550 GeV when  $\Delta m$  is small, between 0.1 – 1.0 GeV, larger values of  $\Delta m$  suppress the relic density due to contribution of electroweak gauge bosons annihilation according to [39]. In the following, we have fixed  $\lambda_L = 0.01$  and  $\Delta m = 1$  GeV.

On the other hand, the desert region for the inert triplet extends up to 1970 GeV. This occurs because of the very small mass splitting ( $\Delta m = 166$  MeV) between the charged  $T^\pm$  and neutral scalars  $T^0$ , which results in a larger annihilation cross section. In addition, we observe that the relic density for the inert triplet is larger when the Higgs portal coupling  $\lambda_{\Phi_1 T} = 0.1$ . For  $\lambda_{\Phi_1 T} = 1.0$ , the relic density is significantly less. Therefore, in order to maximize the relic density for  $T_0$ , we have fixed  $\lambda_{\Phi_1 T} = 0.1$ .

We aim to recover the inert doublet desert region through the contribution of second DM candidate, the inert triplet, which belongs to a different dark sector. In our analysis we have considered  $m_{T^0} > m_{H^0}$ ; the main annihilation channels that contribute to the annihilation cross-section are shown in figure 3. Considering the experimental constraints on the masses of the scalars, the region of interest for each candidate is:  $100 \text{ GeV} \geq m_{H^0} \geq 550 \text{ GeV}$  for the inert doublet and  $100 \text{ GeV} \geq m_{T^0} \geq 2500 \text{ GeV}$  for the inert triplet.

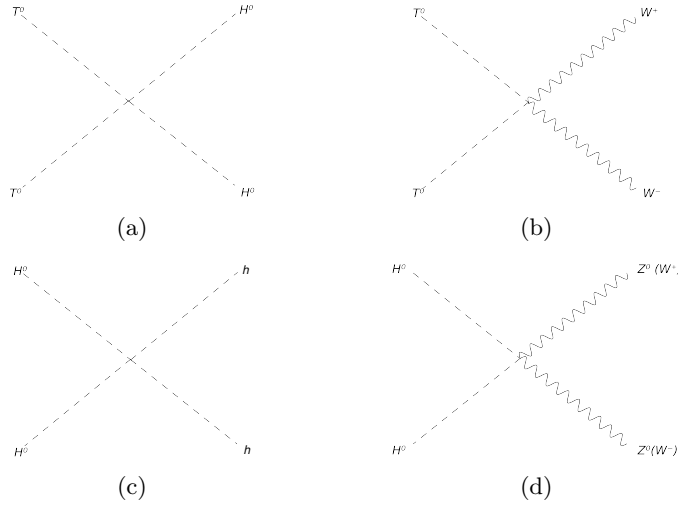


**Fig. 3:** Main annihilation channels contributing to the DM annihilation cross-section for  $m_{T^0} > m_{H^0}$ : (a) DM-DM conversion, (b) DM-W bosons, (c) DM-Higgses and (d) DM- $W^\pm$  bosons ( $Z^0$  bosons)

In order to study the effect of the conversion from  $T^0$  into  $H^0$ , we have computed the relic density for each DM candidate as a function of the mass for different values of  $\lambda_{\Phi_2 T} = \{0, 0.5, 1.0\}$ . In figure 4, we have showed our results for the relic density of each candidate, while maintaining  $M_{T^0} > M_{H^0}$ . The dashed line in each plot represent the Planck limit for the DM over-abundance. We observe that the relic density for

each candidate is again under-abundant for most of the mass range. However, the contribution of both candidates  $\Omega_{Tot}h^2 = \Omega_{H^0}h^2 + \Omega_{T^0}h^2$  satisfies the Planck limit for each value of the  $\lambda_{\Phi_2 T}$  coupling.

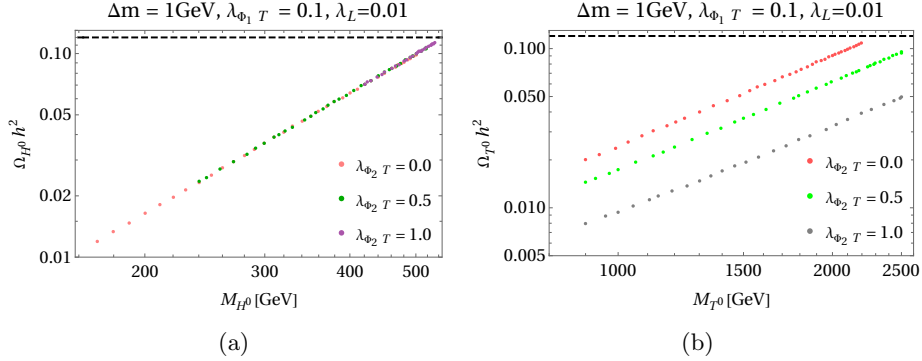


**Fig. 4:** Relic density of (a)  $H^0$  and (b)  $T^0$ , for  $\lambda_{\Phi_2 T} = \{0.0, 0.5, 1.0\}$ ,  $\lambda_L = 0.01$ ,  $\Delta m = 1 \text{ GeV}$  and  $\lambda_{\Phi_1 T} = 0.1$ . The dashed line shows the Planck limit [25] for the relic density of DM. The points satisfy the Planck limit for the total relic density  $\Omega_T h^2$

## 5.2 Direct Detection

In addition to the relic density constraint, we have considered the experimental upper limits for the Spin-Independent (SI) cross-section of DM-nucleons interactions. The corresponding Feynman diagrams for the elastic scattering of DM and nucleons are shown in figure 5. We computed the SI cross-section for each candidate as a function of its mass using micrOMEGAs. In order to compare our results with the experimental limits, we must consider that those limits are based on one-component DM scenarios. Therefore, we need to re-scale the cross section for each component in our model:  $\sigma_{SI}^i * \Omega_i h^2 / \Omega_{Tot} h^2$ , where  $i = H_0, T_0$ . Figure 6 shows the SI cross-section for the DM-nucleon interaction as a function of the mass of each candidate in our model. The different dashed lines indicate the upper experimental limits of the following collaborations: PANDAX-II, XENONnT and LUX-ZEPLIN. The pink and orange shaded regions are excluded by those limits. The solid lines represent our results for different values of  $\lambda_{\Phi_2 T}$ . All points satisfy the theoretical constraints as well as the correct relic density. We observe that our results for both candidates are within the experimental limits. Furthermore, it is worth mentioning our results lie about the neutrino coherent scattering.

In table 2 we have shown some benchmarks allowed by all theoretical and experimental constraints considered. We observe that for the selected values of  $\lambda_{\Phi_2 T}$ , the total relic density  $\Omega_{Tot} h^2$  lies within the Planck limit. All the points allowed by all theoretical and experimental constraints including relic density and direct detection limits are shown in figure 7 in the  $M_{T^0} - M_{H^0}$  plane. We observe that almost the

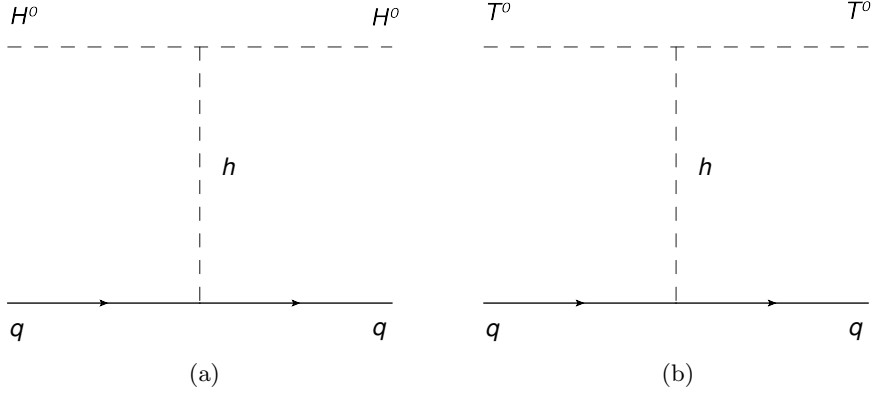


**Fig. 5:** Spin-Independent elastic scattering of DM-nucleon for each candidate

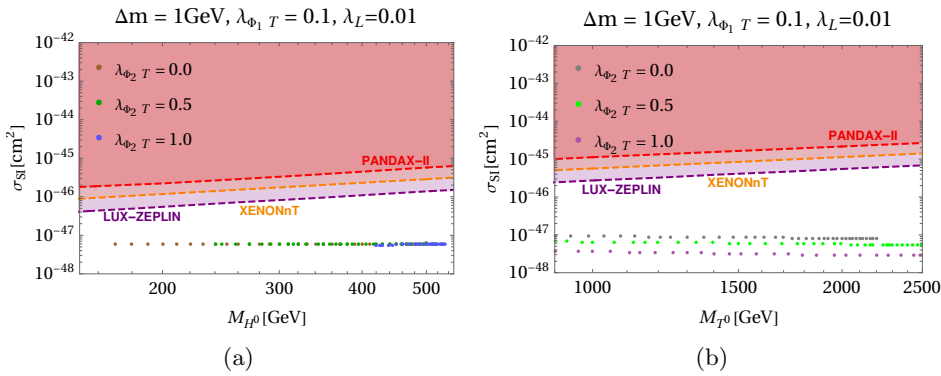


**Fig. 6:** Spin-Independent cross-section of DM-nucleon interaction for (a)  $H^0$  and (b)  $T^0$  for  $\lambda_{\Phi_2 T} = \{0.0, 0.5, 1.0\}$ ,  $\lambda_L = 0.01$ ,  $\Delta m = 1$  GeV and  $\lambda_{\Phi_1 T}$ . Dashed lines represent the limits of PANDAX-II [6], XENONnT [8] and LUX-ZEPLIN [7] experiments. Shaded areas are the regions excluded by those experiments. Points represent our results

entire mass range considered for  $H^0$  is allowed now. On the other hand, the relic density constraint is satisfied for the inert triplet down to  $m_{T^0} \geq 900$  GeV, recovering a significant portion of the desert region ( $m_{T^0} < 1970$  GeV).

## 6 Conclusions

In this work, we have studied a model with an extended scalar sector of the SM that incorporates an inert  $SU(2)_L$  doublet, an inert triplet with  $Y = 0$  and also an active triplet  $\Delta$  with  $Y = 1$ . The DM candidates in this model arise from two dark sectors stabilised by the discrete global symmetries  $\mathbb{Z}_2 \times \mathbb{Z}'_2$ . We have considered a two-component DM scenario to recover the desert regions in the IDM and ITM.

$M_{H^0}$	$M_{T^0}$	$\lambda_{\Phi_2 T}$	$\Omega_{H^0} h^2$	$\Omega_{T^0} h^2$	$\Omega_{\text{Tot}} h^2$	$\sigma_{SI}^{H^0} [pb]$	$\sigma_{SI}^{T^0} [pb]$
170	2200	0.0	$1.20 \times 10^{-2}$	$1.08 \times 10^{-1}$	0.120	$5.892 \times 10^{-11}$	$8.901 \times 10^{-12}$
240	2500	0.5	$2.35 \times 10^{-2}$	$9.51 \times 10^{-2}$	0.119	$2.939 \times 10^{-11}$	$6.830 \times 10^{-12}$
518	900	0.5	$1.07 \times 10^{-1}$	$1.44 \times 10^{-2}$	0.121	$6.852 \times 10^{-12}$	$5.693 \times 10^{-11}$
430	2440	1.0	$7.39 \times 10^{-2}$	$4.74 \times 10^{-2}$	0.121	$9.202 \times 10^{-12}$	$7.182 \times 10^{-12}$
506	1460	1.0	$1.02 \times 10^{-1}$	$1.83 \times 10^{-2}$	0.120	$6.909 \times 10^{-12}$	$2.083 \times 10^{-11}$

**Table 2:** Benchmarks allowed by positivity, perturbativity, unitarity, oblique parameter corrections, relic density and direct detection constraints. The masses are expressed in GeV

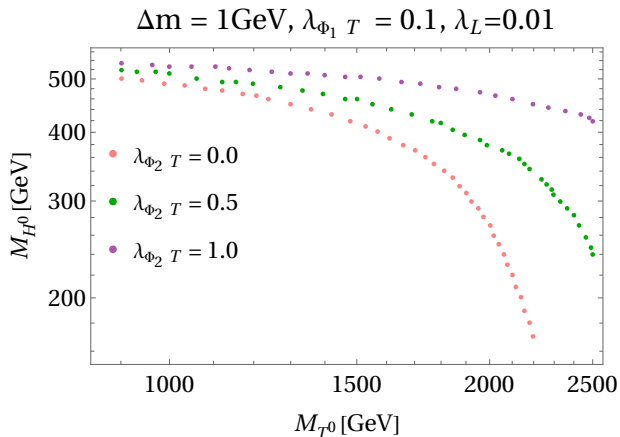


**Fig. 7:** Points allowed by all theoretical constraints that also satisfy the correct relic density and direct detection limits for  $\lambda_{\Phi_2 T} = \{0, 0.5, 1.0\}$

The relevant parameters for the DM phenomenology are the DM candidate masses  $m_{H^0}$ ,  $m_{T^0}$  and the couplings  $\lambda_L$ ,  $\lambda_{\Phi_1 T}$  and  $\lambda_{\Phi_2 T}$ . By considering the experimental constraints on the masses of the scalar and pseudo scalar in the IDM, we have focused on the region  $100 \leq m_{H^0} \leq 550$  GeV for the inert doublet and  $100 \leq m_{T^0} \leq 2500$  for the Inert Triplet. Because the  $\lambda_{\Phi_2 T}$  coupling controls the DM-DM conversion, we computed the relic density for the cases  $\lambda_{\Phi_2 T} = \{0, 0.5, 1.0\}$  for each DM candidate. For both scalars  $H^0$  and  $T^0$ , the relic density is under-abundant such as in the stand-alone cases. However, the contribution of both candidates allow us to obtain the correct total relic density for  $M_{H^0} \geq 170$  GeV and  $M_{T^0} \geq 900$  GeV as shown in table 2 and figure 7. We have successfully recovered about 84% of the desert region for  $H^0$  and about 57% of the desert region for  $T^0$ . We also considered the upper bounds for the SI cross-section for DM-nucleon interactions, our results for both candidates are within the experimental limits of PANDAX-II and XENONnT and LUX-ZEPLIN collaborations.

In addition to the study of DM phenomenology, we have shown that it is possible to generate the light neutrino masses in our model through the seesaw type-II mechanism. A small VEV  $v_\Delta \sim 1$  eV of the  $\Delta$  triplet is required. It is worth mentioning that

it is possible to generate matter-antimatter asymmetry in our model via leptogenesis, through the CP-violating decays of the active scalar triplet into leptons  $\Delta \rightarrow \bar{\ell}\ell$  as shown in [23]. This will be studied in a further work.

## 7 Acknowledgments

This work has been funded by PAPIIT project No IN102122. JML would like to thank the DGAPA-UNAM Postdoctoral grant. SMD would like to thank Consejo Nacional de Humanidades Ciencia y Tecnología (CONAHCYT) Doctorate grant. RG and JML thank to Sistema Nacional de Investigadores (SNI) of the Consejo Nacional de Humanidades, Ciencia y Tecnología (CONAHCYT) in México.

## Data Availability Statement

No Data associated in the manuscript.

## References

- [1] Glashow, S.L.: Partial symmetries of weak interactions. *Nucl. Phys.* **22**(4), 579–588 (1961)
- [2] A. Salam, J.C.W.: Electromagnetic and weak interactions. *Phys. Lett.* **13**(2), 168–171 (1964)
- [3] Weinberg, S.: A Model of Leptons. *Phys. Rev. Lett.* **19**(21), 1264 (1967)
- [4] (Super Kamiokande Collaboration), Y.F.: Evidence for Oscillation of Atmospheric Neutrinos. *Phys. Rev. Lett.* **81**(8), 1562 (1998)
- [5] V.C. Rubin, W.K.F.J.: Rotation of the Andromeda Nebula from a Spectroscopic Survey of Emission Regions. *Astrophys. J.* **159**, 379–403 (1970)
- [6] (PANDA Collaboration), X.C.: Dark Matter Results from 54-Ton-Day Exposure of PandaX-II Experiment. *Phys. Rev. Lett.* **119**(18), 181302 (2017)
- [7] (LUX-ZEPLIN Collaboration), J.A.: First Dark Matter Search Results from the LUX-ZEPLIN(LZ) Experiment. *Phys. Rev. Lett.* **131**(4), 041002 (2023)
- [8] Aprile, E.e.a.: First dark matter search with nuclear recoils from the xenonnt experiment. *Phys. Rev. Lett.* **131**, 041003 (2023) <https://doi.org/10.1103/PhysRevLett.131.041003>
- [9] Taoso, M., Bertone, G., Masiero, A.: Dark Matter Candidates: A Ten-Point Test. *JCAP* **03**, 022 (2008) <https://doi.org/10.1088/1475-7516/2008/03/022> [arXiv:0711.4996](https://arxiv.org/abs/0711.4996) [astro-ph]

- [10] L. L. Honorez, C.E.Y.: The inert doublet model of dark matter revisited. High Energ. Phys. **46**(9) (2010)
- [11] M. Krawczyk, D.S. N. Darvishi: The Inert Doublet Model and its extensions. arXiv:1512.06437v2 [hep-ph] (2015)
- [12] M. A. Arroyo-Ureña, R. Gaitán, R. Martínez, J.H. Montes de Oca Yemha: Dark matter in inert doublet model with one scalar singlet and  $U_x(1)$  gauge symmetry. Eur. Phys. J. C **80**(8), 788 (2020)
- [13] Kalinowski, J., Kotlarski, W., Robens, T., Sokolowska, D., Żarnecki, A.F.: The inert doublet model at current and future colliders. J. Phys.: Conf. Ser. **1586**(1), 012023 (2020) <https://doi.org/10.1088/1742-6596/1586/1/012023>
- [14] Ma, E.: Verifiable radiative seesaw mechanism of neutrino mass and dark matter. Phys. Rev. D **73**, 077301 (2006) <https://doi.org/10.1103/PhysRevD.73.077301>
- [15] Fischer, O., Bij, J.J.: Multi-singlet and singlet-triplet scalar dark matter. Mod. Phys. Lett. **26**(27), 2039–2049 (2011)
- [16] Araki, T., Geng, C.Q., Nagao, K.I.: Dark matter in inert triplet models. Phys. Rev. D **83**, 075014 (2011) <https://doi.org/10.1103/PhysRevD.83.075014>
- [17] Khan, N.: Exploring the hyperchargeless Higgs triplet model up to the Planck scale. Eur. Phys. J. C **78**(4), 341 (2018) <https://doi.org/10.1140/epjc/s10052-018-5766-4> arXiv:1610.03178 [hep-ph]
- [18] Chakrabarty, N., Roshan, R., Sil, A.: Two-component doublet-triplet scalar dark matter stabilizing the electroweak vacuum. Phys. Rev. D **105**, 115010 (2022) <https://doi.org/10.1103/PhysRevD.105.115010>
- [19] Betancur, A., Castillo, A., Palacio, G., Suarez, J.: Multicomponent scalar dark matter at high-intensity proton beam experiments. Journal of Physics G: Nuclear and Particle Physics **49**(7), 075003 (2022) <https://doi.org/10.1088/1361-6471/ac65a6>
- [20] (CMS Collaboration), S.C.: Observation of a new boson at a mass of 125 gev with the cms experiment at the lhc. Physics Letters B **716**(1), 30–61 (2012) <https://doi.org/10.1016/j.physletb.2012.08.021>
- [21] Cirelli, M., Strumia, A.: Minimal dark matter: models and results. New J. Phys. **11**, 105005 (2009)
- [22] Mohapatra, R.N.: Neutrino mass - an overview. Nucl. Phys. B - Proceedings Supplements **138**, 257–266 (2005) <https://doi.org/10.1016/j.nuclphysbps.2004.11.061> . Proceedings of the Eighth International Workshop on Topics in Astroparticle and Underground Physics



- [23] Datta, A., Roshan, R., Sil, A.: Scalar triplet flavor leptogenesis with dark matter. *Phys. Rev. D* **105**, 095032 (2022) <https://doi.org/10.1103/PhysRevD.105.095032>
- [24] (Particle Data Group), R.W.: Review of Particle Physics. *Prog. of Theor. Exp. Phys.* **2022**(8) (2022) <https://doi.org/10.1093/ptep/ptac097> <https://academic.oup.com/ptep/article-pdf/2022/8/083C01/49175539/ptac097.pdf>. 083C01
- [25] (Planck Collaboration), N.A.: Planck 2018 results. *A&A* **641**(A6), 67 (2020)
- [26] Lundström, E., Gustafsson, M., Edsjö, J.: Inert doublet model and lep ii limits. *Phys. Rev. D* **79**, 035013 (2009) <https://doi.org/10.1103/PhysRevD.79.035013>
- [27] M. Krawczyk, P.S. D. Sokolowska, Świeżewska, B.: Constraining inert dark matter by  $r_{\gamma\gamma}$  and wmap data. *JHEP* **2013**(9), 55 (2013)
- [28] OPAL Collaboration, G.A.e.a.: Search for chargino and neutralino production at  $\sqrt{s} = 192$  GeV to 209 GeV at LEP. *Eur. Phys. J. C* **35**(1), 1–20 (2004)
- [29] Pierce, A., Thaler, J.: Natural dark matter from an unnatural higgs boson and new colored particles at the tev scale. *JHEP* **2007**(08), 026 (2007) <https://doi.org/10.1088/1126-6708/2007/08/026>
- [30] (CMS Collaboration), A.M.S.: Combined measurements of Higgs boson couplings in proton-proton collisions at  $\sqrt{s} = 13$  TeV. *Eur. Phys. J. C* **79**(5), 421 (2019)
- [31] Kannike, K.: Vacuum stability conditions from copositivity criteria. *Eur. Phys. J. C* **72**(7), 2093 (2012)
- [32] Ginzburg, I.F., Ivanov, I.P.: Tree-level unitarity constraints in the most general two higgs doublet model. *Phys. Rev. D* **72**, 115010 (2005) <https://doi.org/10.1103/PhysRevD.72.115010>
- [33] Peskin, M.E., Takeuchi, T.: Estimation of oblique electroweak corrections. *Phys. Rev. D* **46**, 381–409 (1992) <https://doi.org/10.1103/PhysRevD.46.381>
- [34] Grimus, W., Lavoura, L., OGREID, O.M., OSLAND, P.: The oblique parameters in multi-higgs-doublet models. *Nucl. Phys. B* **801**(1), 81–96 (2008) <https://doi.org/10.1016/j.nuclphysb.2008.04.019>
- [35] Forshaw, J.R., White, B.E., Ross, D.A.: Higgs mass bounds in a triplet model. *JHEP* **2001**(10), 007 (2001) <https://doi.org/10.1088/1126-6708/2001/10/007>
- [36] Cheng, Y., He, X.-G., Huang, F., Sun, J., Xing, Z.-P.: Electroweak precision tests for triplet scalars. *Nucl. Phys. B* **989**, 116118 (2023) <https://doi.org/10.1016/j.nuclphysb.2023.116118>
- [37] Staub, F.: Sarah 4: A tool for (not only susy) model builders. *Comp. Phys. Comm.*

**185**(6), 1773–1790 (2014) <https://doi.org/10.1016/j.cpc.2014.02.018>

- [38] Bélanger, G., Boudjema, F., Pukhov, A., Semenov, A.: micromegas4.1: Two dark matter candidates. *Computer Physics Communications* **192**, 322–329 (2015) <https://doi.org/10.1016/j.cpc.2015.03.003>
- [39] Sarma, L., Das, P., Das, M.K.: Scalar dark matter and leptogenesis in the minimal scotogenic model. *Nucl. Phys. B* **963**, 115300 (2021) <https://doi.org/10.1016/j.nuclphysb.2020.115300>